Supporting Information

Mass Transport Control over Conductive MOF 3D Thin Film to Improve Gas Sensing

Yu Pan[ac+], Wei Sun[a+], Junxiang Chen[a], Yuan Lin[a], Yong-Jun Chen[ab]*, Zhenhai Wen[a]* and Gang Xu[abc]*

[a]State Key Laboratory of Structural Chemistry, and Fujian Provincial Key Laboratory of Materials and Techniques toward Hydrogen Energy, Fujian Institute of Research on the Structure of Matter, Chinese Academy of Sciences, Fuzhou 350002, China.

[b]Fujian Science & Technology Innovation Laboratory for Optoelectronic Information of China Fuzhou, Fujian 350108 (China).

[c]University of Chinese Academy of Sciences (UCAS) Beijing 100049 (P. R. China)

[†]These authors contributed equally to this paper.

Corresponding author: (Y. J. Chen: chenyongjun@fjirsm.ac.cn; Z. Wen: Wen@fjirsm.ac.cn; G. Xu: gxu@fjirsm.ac.cn).

Materials

All reagents were purchased commercially and used without further purification. Zinc acetate dihydrate ($Zn(Ac)_2 \cdot 2H_2O$), hexamethylenetetramine (HMT) and copper acetate monohydrate ($Cu(OAc)_2 \cdot H_2O$) were purchased from Aladdin, (Shanghai), China; HHTP (2, 3, 6, 7, 10, 11-hexahydrotriphenylene) ligand was purchased from TCI (Shanghai), China; Concentrated hydrochloric acid (36% ~ 38% by weight) was purchased from Sino pharm Group, China; (001) Sapphire substrates ($8 \times 10 \times 1$ mm^3) were purchased from Jinan Optoelectronics Co., Ltd., China.

Experimental Section/Methods

Finite element method simulation: In reference to all the models, we consistently employ the Fick's diffusion law.

$$\frac{\partial c_i}{\partial t} + \nabla \cdot J_i + u \cdot \nabla c_i = 0 \quad (1)$$

$$J_i = -D_i \nabla c_i \quad (2)$$

To address the diffusion problem of gas in a nanowire system, we consider the variables where c_i represents the concentration of the gas, J_i denotes the system's flux, and D_i is the diffusion coefficient. It is important to note that previous literature often employs Darcy's Law for solving the flow of gases. These two equations are mathematically equivalent: in Fick's diffusion law, the diffusion coefficient D_i is a constant inversely proportional to the kinetic viscosity coefficient, and its concentration gradient corresponds to the gas pressure gradient in Darcy's Law. In simulations, at t = 0, the gas concentration is only 1 mol m^{-3} (approximately 0.02 atm when calculated as an ideal gas) at the inlet and zero elsewhere. Within the gas chamber, the diffusion coefficients for the non-slip region and inside the MOF are set at 3×10^{-13} m^2 s^{-1}, 1×10^{-16} and 1×10^{-17} m^2 s^{-1}, respectively. These values are derived from the following calculations: we used DFT based Nudged Elastic Band to calculate the migration energy barrier $\Delta G^{\#}$ for NH_3 at the interface sites in MOF, which is approximately 0.7 eV. With a diffusion distance L of about 4 Å, the diffusion coefficient can be calculated using the transition state theory $D = k_0 L^2 = L^2 \left(\frac{k_B T}{\hbar}\right) \exp\left(\frac{-\Delta G^{\#}}{RT}\right)$, resulting in a diffusion coefficient of approximately 1E-17 m²/s. The diffusion coefficients for the non-slip surface and bulk regions are taken from literature[1], approximately 10 and 3E4 times the diffusion coefficient in MOF, respectively.

Additionally, regarding off-axis laminar flow and possible turbulent flow in the model:

About the former, we have supplemented the discussion with the impact of off-axis laminar flow on gas flow, as shown in **Figure S2**. The results indicate that its impact is relatively minor. About the latter, we roughly calculated the Reynolds number ($Re = \rho u L/\mu$) using the gas density ρ = 0.695 kg/m³, dynamic viscosity $\mu \approx$ 0.99E-5 Pa·s, flow velocity $u \approx$ 1E-8 m/s, and characteristic length L = 5E-6 m. The calculated Reynolds number is much lower than 2000, indicating the absence of turbulent flow.

Preparation of ZnO-NWAs template: Sapphire substrates were ultrasonically washed using deionized water, acetone and ethanol for 10 min. A layer of ZnO seeds was deposited on the surface of sapphire substrates by spin-coating a methanol solution of 0.01 M zinc acetate and calcination in a tube furnace at 350 °C for 30 min. Then the substrate was up-down dipped into a mixture aqueous solution of 8 mL aqueous solution of zinc acetate dihydrate ($Zn(Ac)_2{\cdot}2H_2O$) and 8 mL aqueous solution of hexamethylenetetramine (HMT) in a sealed autoclave with a stainless steel shell at 95°C inside an oven. After that, the substrates were washed repeatedly with DI-water and pure ethanol alternately and then annealed in a tube furnace at 550 °C for 2 h. Moreover, by adjusting the concentration of the ZnO precursor solution and the time of the hydrothermal reaction, ZnO-NWAs with different densities and lengths can be obtained.

Table S1 Preparation of ZnO-NWAs with different density

Density	Concentration of $Zn(Ac)_2{\cdot}2H_2O$	Concentration of HMT	Reaction time
70 %	0.01 M	0.01 M	16 h
85 %	0.015 M	0.016 M	16 h
90 %	0.02 M	0.02 M	16 h
95 %	0.03 M	0.03 M	16 h

Table S2 Preparation of ZnO-NWAs with different height

Height	Concentration of $Zn(Ac)_2{\cdot}2H_2O$	Concentration of HMT	Reaction time
1 μm	0.03 M	0.03 M	1 h
2 μm	0.02 M	0.02 M	10 h
3μm	0.015 M	0.015 M	16 h

Synthesis of 3D Cu-HHTP 3D thin film*:* Cu-HHTP 3D thin films were grown on ZnO-NWAs template using the layer-by-layer (LBL) and liquid-phase epitaxy (LPE) method at 35 °C. Cu-HHTP 3D thin films were prepared using the following dilute ethanol solutions: $Cu(OAc){\cdot}H_2O$ (0.1 mM) and HHTP (0.01 mM). The ZnO-NWAs templates were alternatively soaked in $Cu(OAc)_2{\cdot}H_2O$ and HHTP solutions for 10 and 20 minutes in the first cycle, respectively, and alternatively soaked in $Cu(OAc)_2{\cdot}H_2O$ and HHTP solutions for 5 and 10 minutes in the subsequent each repeating cycle, respectively. The thin films were washed with pure ethanol to remove residual reactants in each repeating growth cycle. Finally, the thin films were dried naturally at room temperature. By controlling the number of growth cycles (6 C for 5 nm, 10 C for 20 nm, 15 C for 35 nm), Cu-HHTP 3D thin films with different thicknesses were successfully obtained. Cu-HHTP 3D thin films with different height and density were obtained by replacing ZnO-NWAs templates with different heights and array densities using the same method.

***Gas sensor characterizations**:* Chemiresistive sensors of Cu-HHTP 3D thin film were fabricated using silver paste as the electrode, and 50 μm diameter gold wire attached on the silver paste as the conducting wires. A pair of parallel electrodes were connected to both ends of the thin films where only Cu-HHTP was grown on a sapphire substrate. The sensors were measured in a home-made sensing system that has been reported in our previous work. The sensor devices were placed in an opaque sealed quartz chamber at room temperature and dry air was used as the carrier gas for the target gas. The DC current changes of the device under different concentrations of target gas were monitored to conduct gas sensing experiments. The sensor devices were measured using a DC circuit with an applied bias of 5 V using a Keithley 2602B (USA) source meter. Target gas was introduced into the quartz tube by mixing the certified gas ''mixtures'' (Beijing Hua Yuan Gas Chemical Industry Co., Ltd., China) and mixed air (dry air) in a proper ratio controlled by the mass flow controllers (CS-200C, Beijing Sevenstar Quali-flow Electronic Equipment Manufacturing Co., Ltd., China). The constant flow was 200 mL min^{-1}. All of the sensing measurements were performed at ambient conditions.

The sensor response with positive response is defined as the ratio of sensor resistance in air (R_0) and in analytic gas (R_{gas}):

$$\text{Response} = R_0/R_{gas} - 1$$

The sensor response with negative response is defined as the ratio of R_{air} and $R_{analyte}$:

$$\text{Response} = R_{gas}/R_0 - 1$$

Characterization: Scanning electron microscope (SEM, ZEISS-300) was operated at 5.0 kV. Transmission electron microscope (TEM) images were obtained on a JEOL-2010 transmission electron microscope at an acceleration voltage of 200 kV. Powder X-ray diffraction (PXRD) patterns were recorded with a Rigaku Smartlab X-ray diffractometer equipped with a 1D array detector using Cu Kα radiation (λ = 1.54178 Å). The step size was set as 0.02°. Fourier transform infrared spectroscopy (FT-IR) spectra were recorded on a Bruker VERTEX70 FT-IR spectrometer (Germany) in 4000 – 600 cm^{-1} regions using KBr pellets. *I–V* curves of materials at room temperature were measured by a Keithley 4200 (USA) semiconductor characterization system via a two-probe DC method.

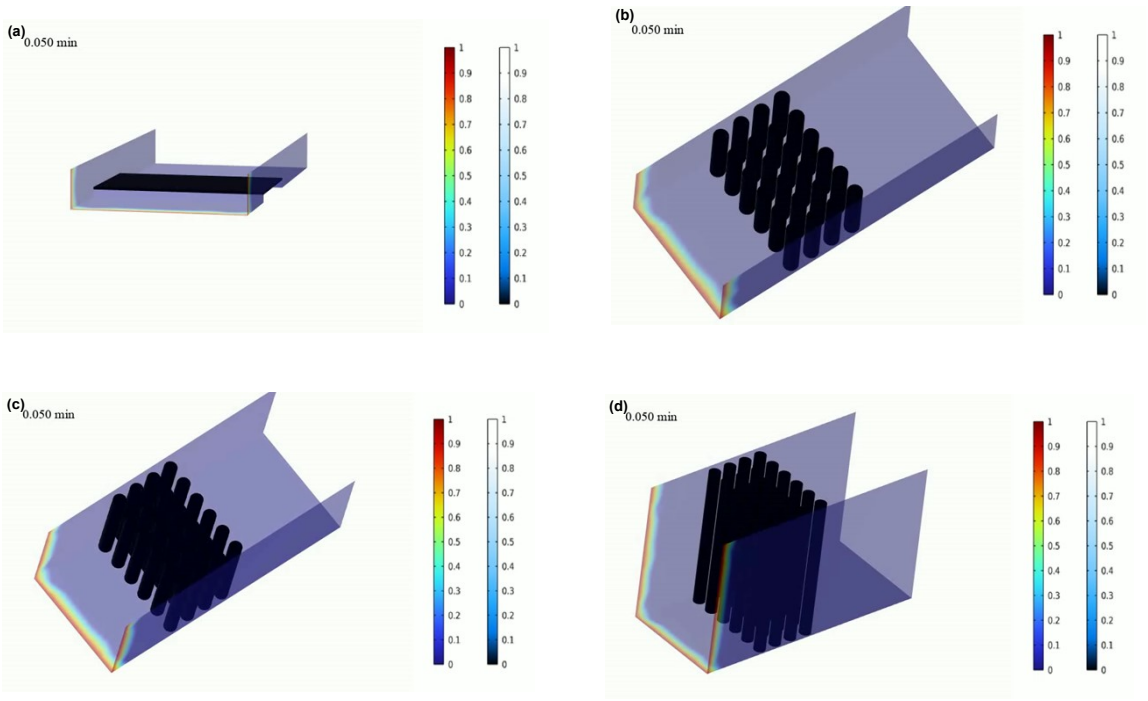

Audio Video Interactive S1: The relationships between MOF 2D thin flim (a) and MOF 3D thin films with height of 1 µm (b), 2 µm (c), and 3 µm (d), and the time-varying molecular adsorption quantities.

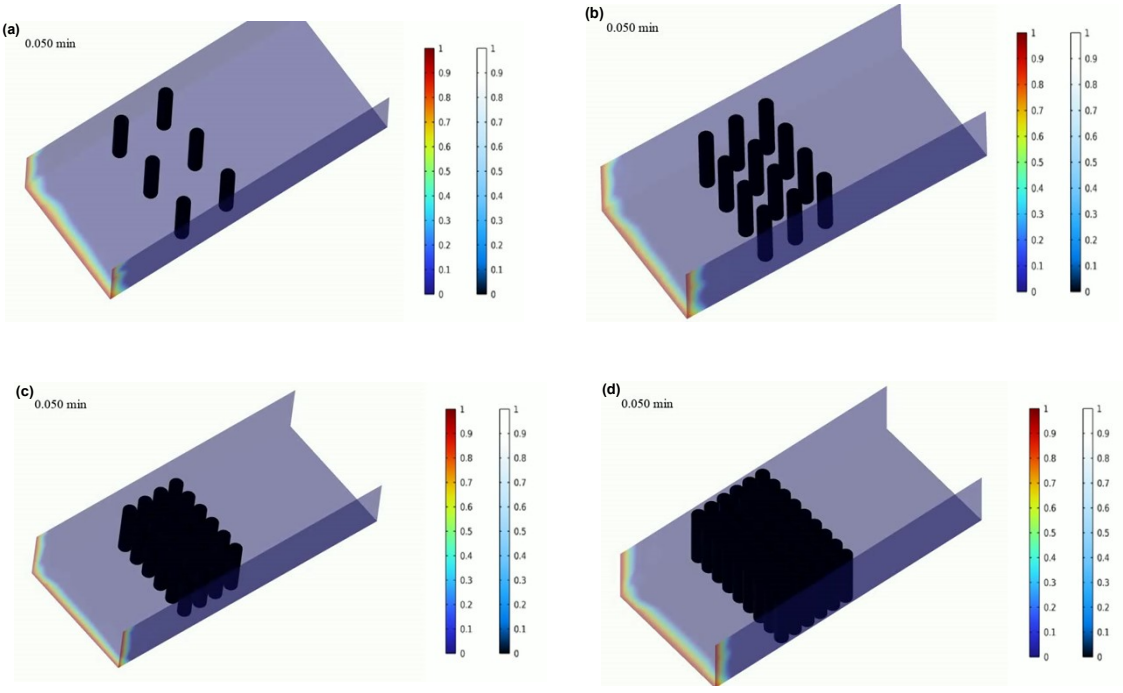

Audio Video Interactive S2: The relationships between MOF 3D thin films with different densities and the time-varying molecular adsorption quantities.

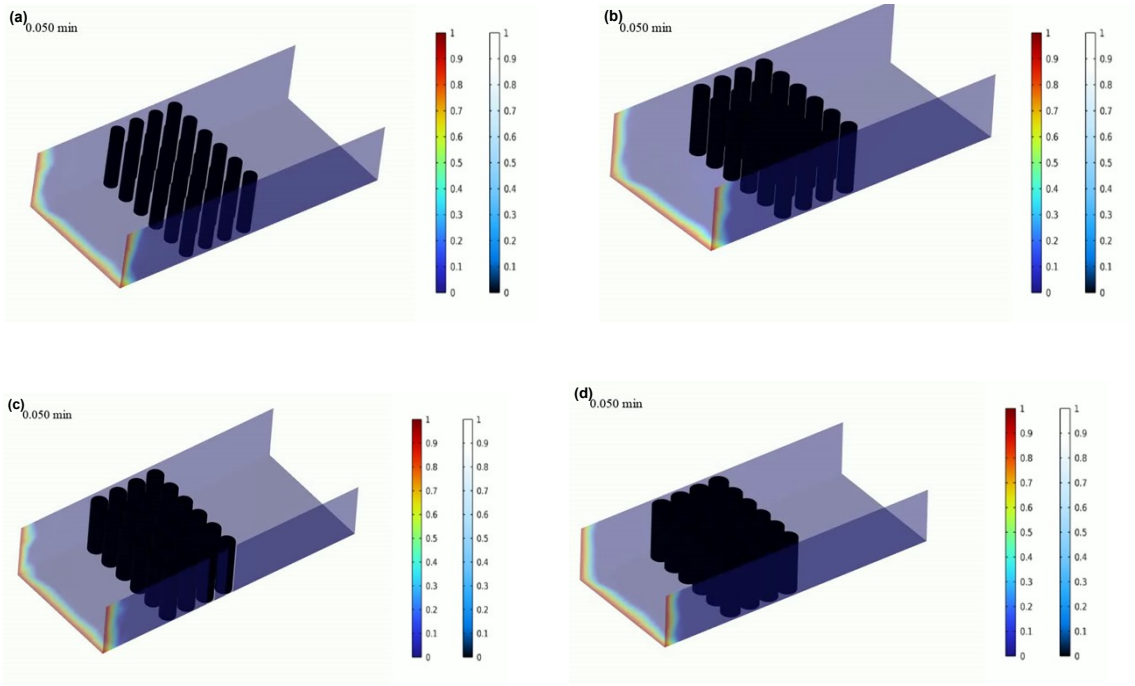

Audio Video Interactive S3: The relationships between MOF 3D thin films different thicknesses and the time-varying molecular adsorption quantities.

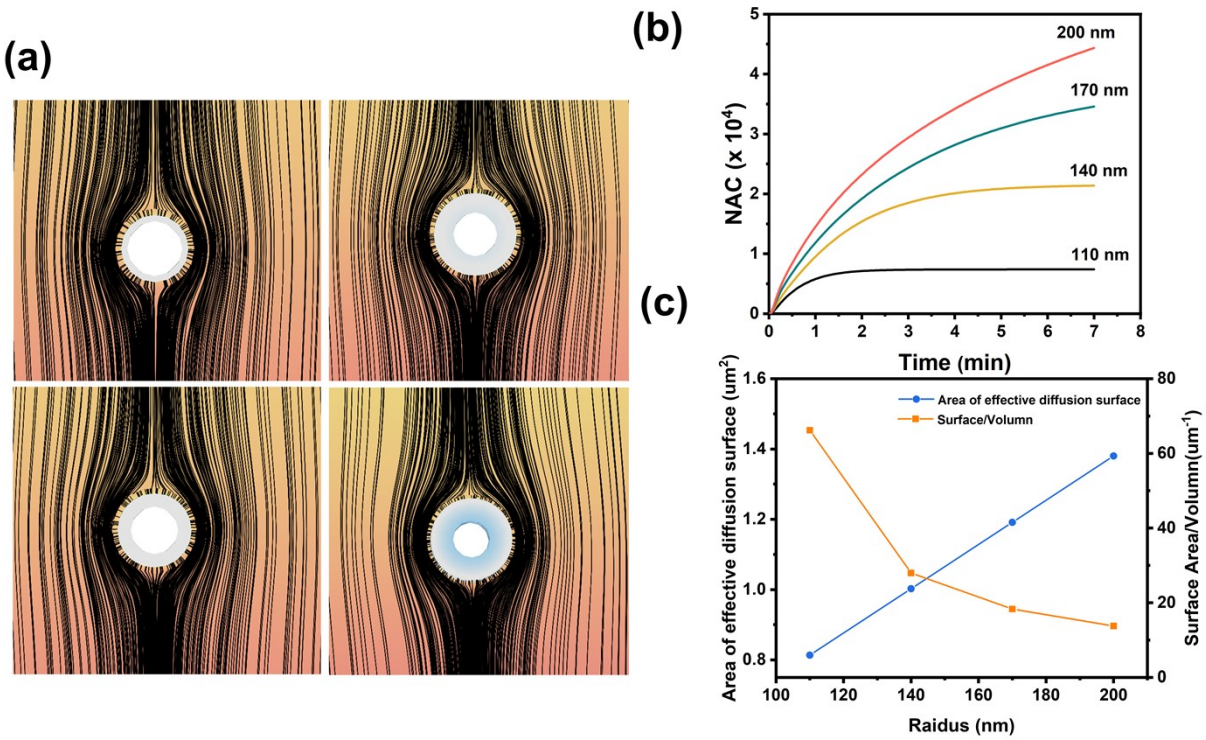

Figure S1 (a) Schematic diagram of the simulated structure. (b) time-dependent molecular capture quantities of different radius of nano rod. (c) The dependence of Area of effective diffusion surface and surface Area to the radius of nano rod.

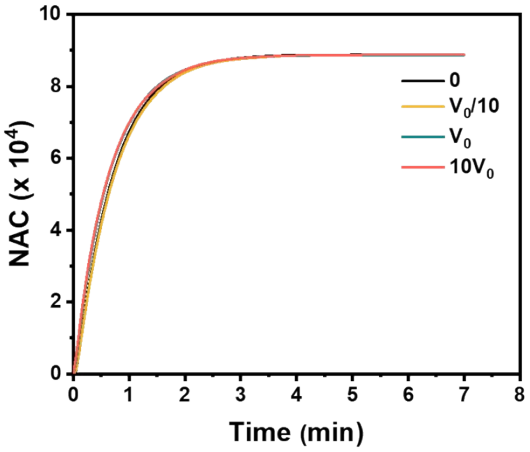

Figure S2. Time-dependent molecular capture quantities under different off-axis laminar flow. One can see the impact is negligible.

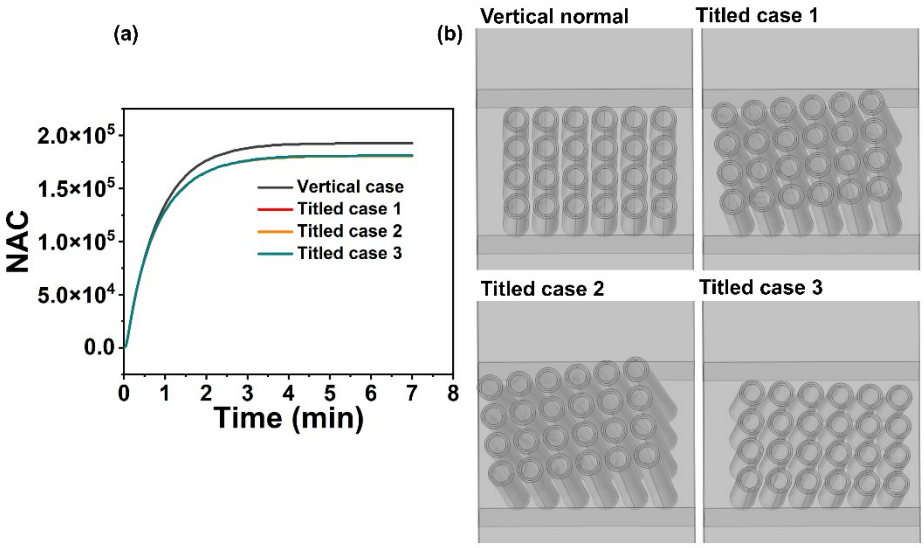

Figure S3 (a) The time-dependent molecular capture quantities in the system, (b) models with different cases.

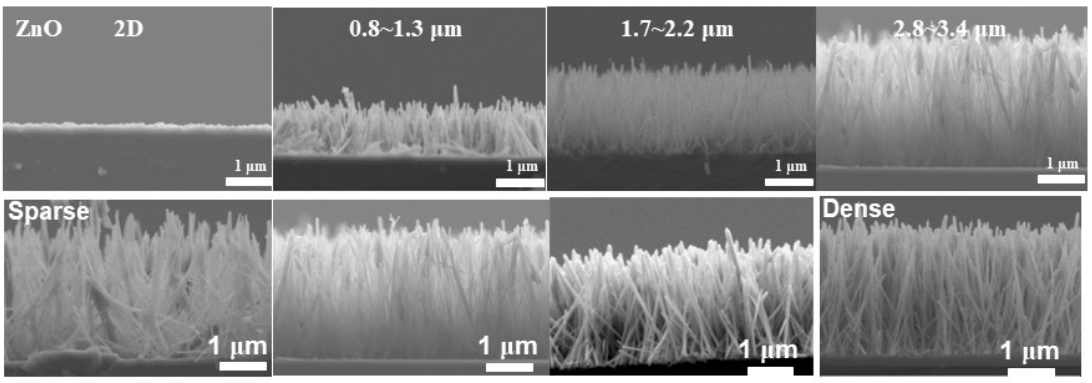

Figure S4. SEM images of ZnO-NWAs template.

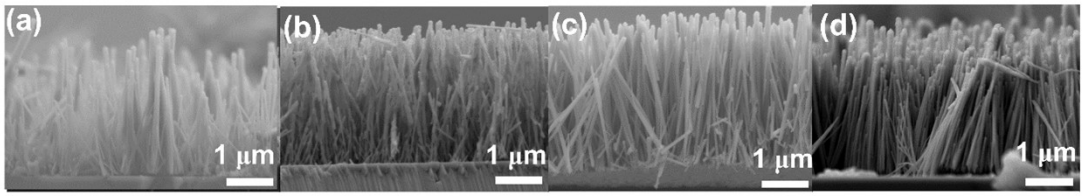

Figure S5. SEM images of Cu-HHTP 3D thin films grown on ZnO-NWAs substrate with different densities.

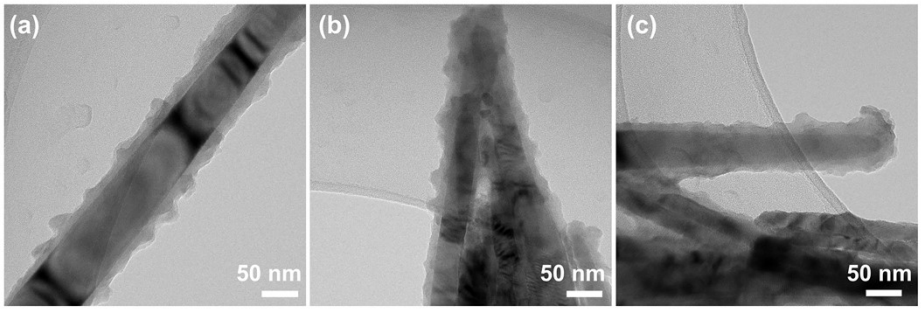

Figure S6. TEM of 20 nm Cu-HHTP 3D thin films with 70% (a), 90% (b) and 95% (c) densities.

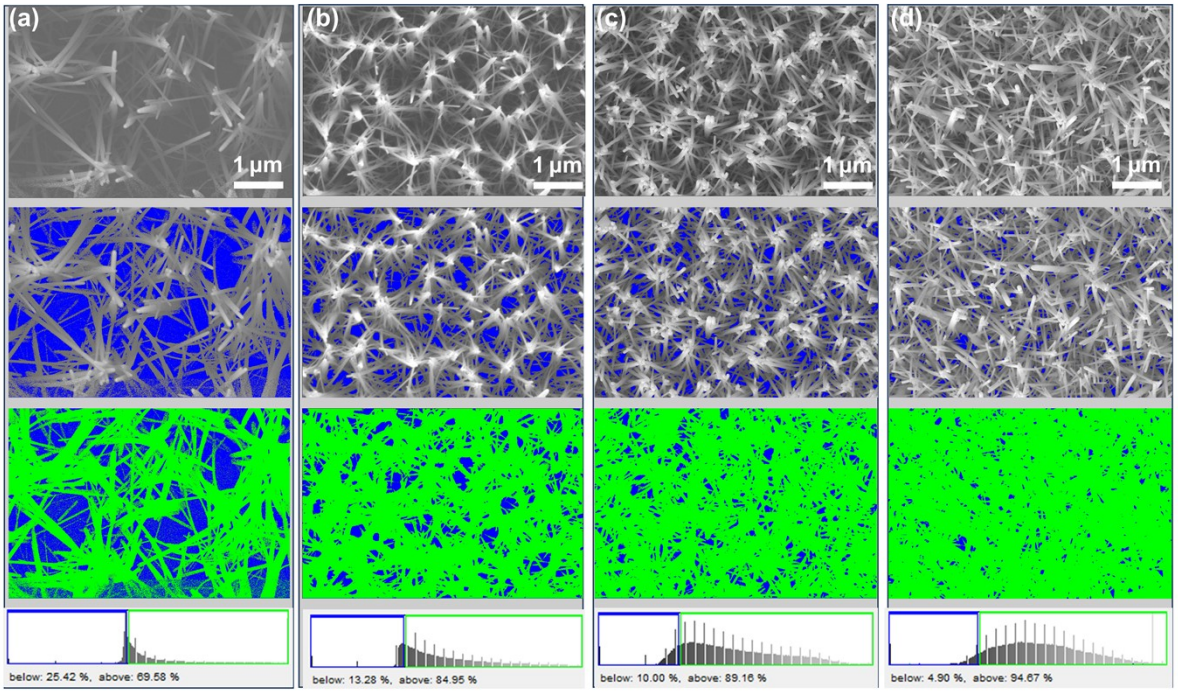

Figure S7. The detail of how the density of 70% (a), 85 (b), 90% (c) and 95% (d) were measured by Image J.

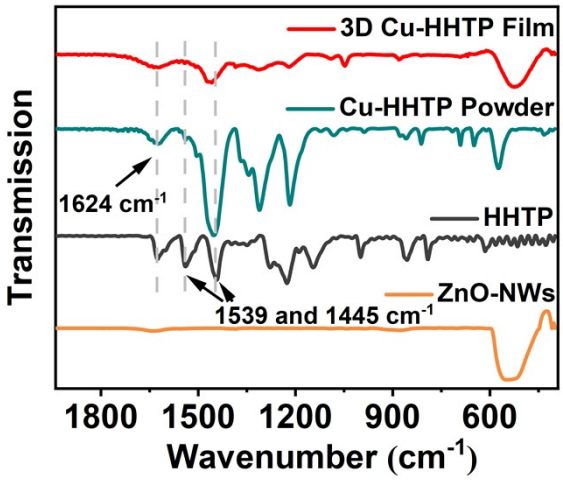

Figure S8. FT-IR of 3D Cu-HHTP thin film, Cu-HHTP powder, HHTP and ZnO-NWAs.

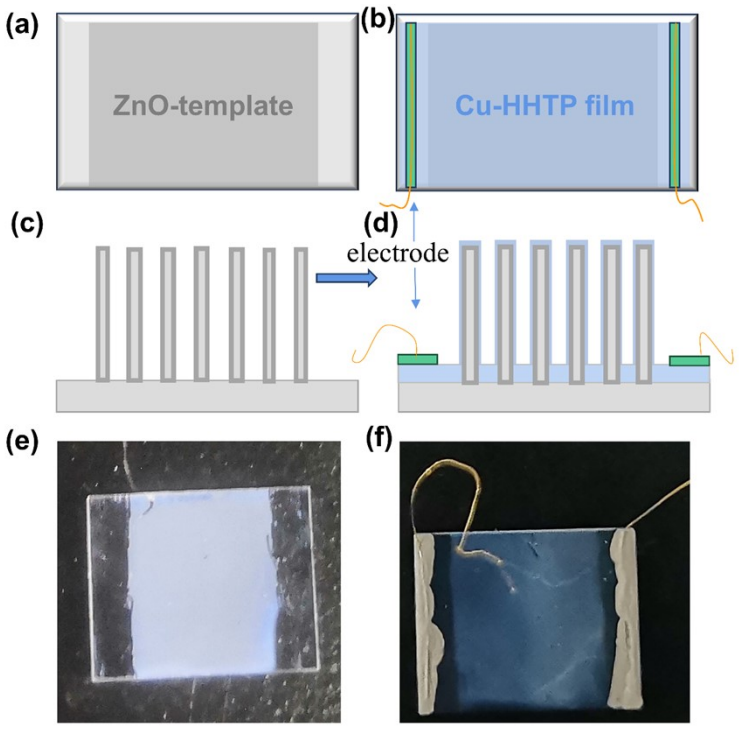

Figure S9. (a) Scheme of the top view (a, b) and side view (c, d) of the device preparation; Photo of (e) ZnO-NWA template and (f) device of Cu-HHTP 3D thin film grown on ZnO-NWA template.

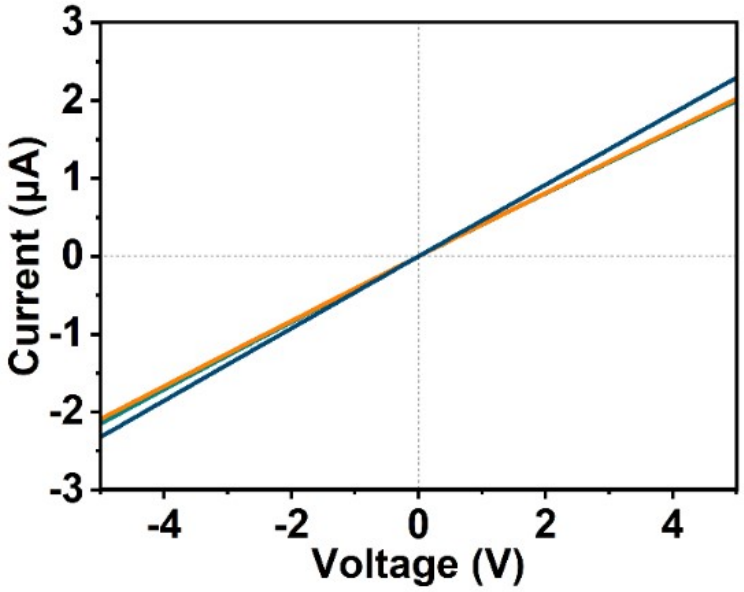

Figure S10. *I-V* curves of ZnO-NWAs.

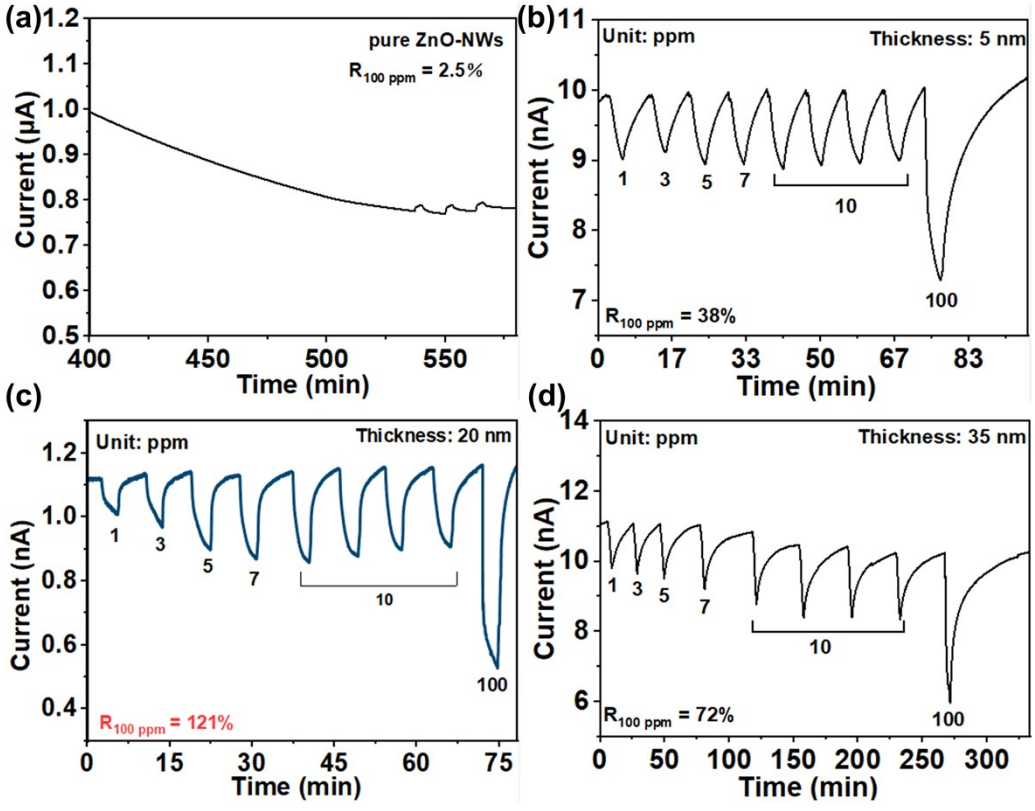

Figure S11. (a) Response–recovery curve of pure ZnO-NWA to 100 ppm NH_3; Response–recovery curve of Cu-HHTP 3D thin film with thickness of 5 nm (b), 20 nm (c) and 35 nm (d), height of ~3 μm and density of 85% toward different concentration of NH_3 (The different numbers under the curve represent different concentrations of ammonia obtained by mixing 100 ppm with dry air in different proportions).

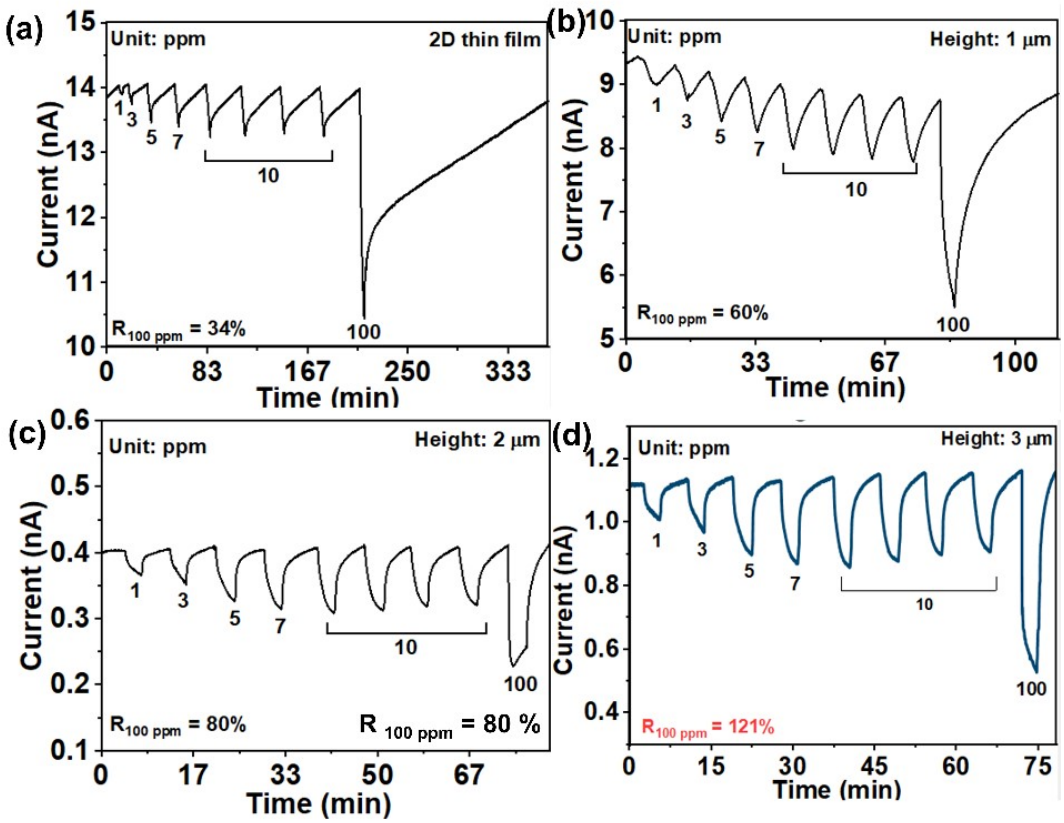

Figure S12. Response–recovery curve of Cu-HHTP 3D thin film with thickness of 20 nm, height of ~0.05 μm (a), 1 μm (b), 2 μm (c) 3 μm (d) and density of 85% toward different concentration of NH_3 (The different numbers under the curve represent different concentrations of ammonia obtained by mixing 100 ppm with dry air in different proportions).

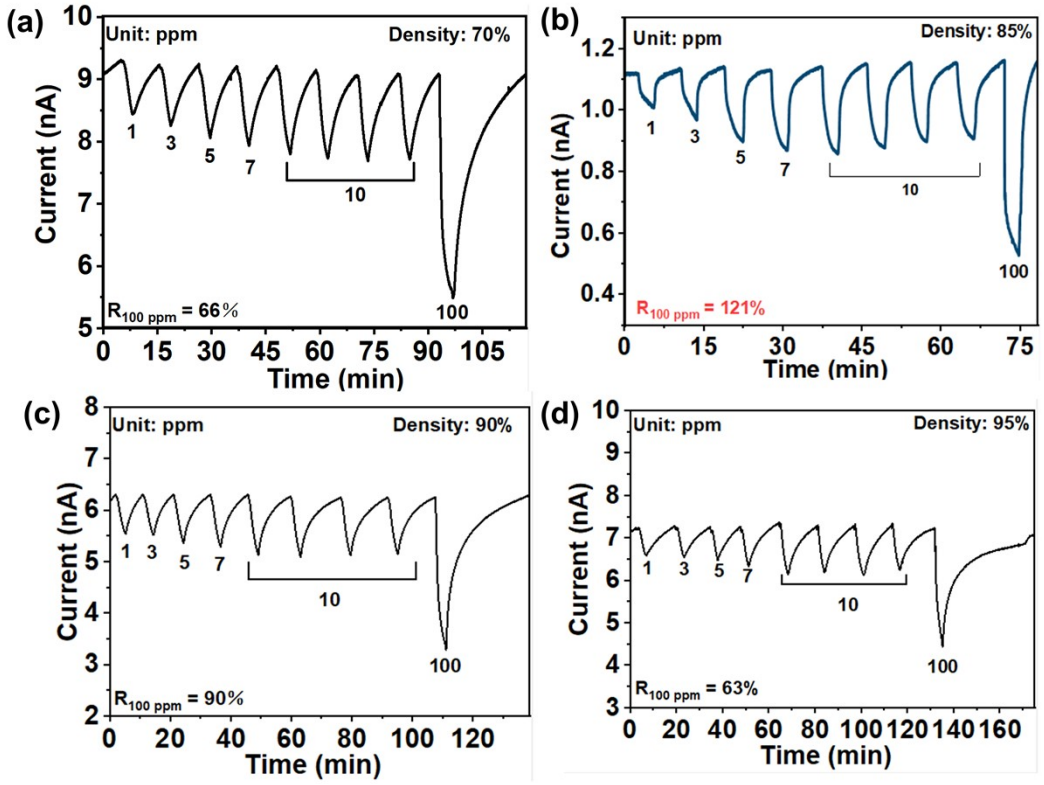

Figure S13. Response–recovery curve of Cu-HHTP 3D thin film with thickness of 20 nm, height of ~3 µm and density of 70% (a), 85% (b), 90% (c) and 95% (d) toward different concentration of NH_3 (The different numbers under the curve represent different concentrations of ammonia obtained by mixing 100 ppm with dry air in different proportions).

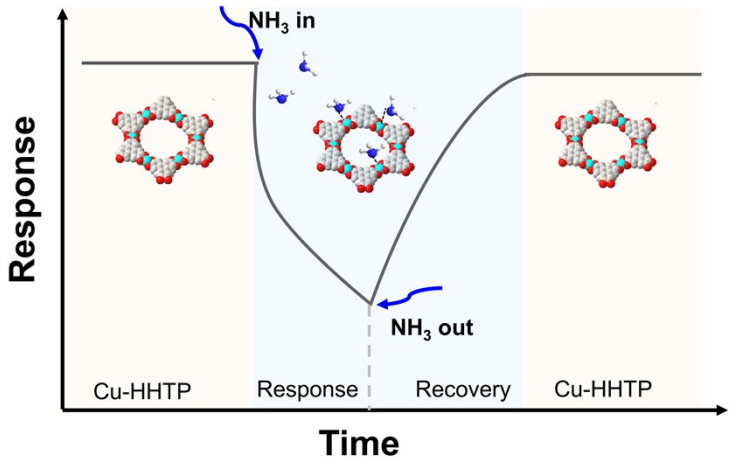

Figure S14. Proposed sensing mechanism of Cu-HHTP 3D thin film in response to NH_3

Table S3: Room-temperature gas sensing performance of various chemiresistive materials toward NH_3.

Material	Response /%	LOD	Ref.
Cu-HHTP-3D film	121 (100 ppm)	0.78 ppm	This work
Cu-HHTP-3D film	161 (100 ppm)	87 ppt	2
Cu-HHTP-film	129 (100 ppm)	0.5 ppm	3
Cu-HHTP-THQ	15 (100 ppm)	0.02 ppm	4
Zn-HHTP-H film	40.5 (50 ppm)	39.9 ppb	
PcCu-Zn-H film	61.8 (100 ppm)	-	4
Co-HHTP-H film	8.86 (20 ppm)	-	4
COF-DC-8	39 (40 ppm)	57 ppb	5
HMP-TAPB-1	70 (50 ppm)	1 ppm	6
Cu-BTC@GO	7 (500 ppm)	100 ppm	7
NiPc-Ni	43 (80 ppm)	0.05 ppm	8
NiPc-Cu	45 (80 ppm)	0.05 ppm	8
Cu-BHT	15 (100 ppm)	0.23 ppm	9
CuTCNQ	5 (99 ppm)	10 ppm	10
Cu_3HITP_2	2.6 (10 ppm)	0.5 ppm	11
CuPc@IRMOF-3	100 (50 ppm)	52 ppb	12
Polypyrrole nanotubes	200 (2 ppm)	50 ppt	13
V_2O_3 nanosheet	2.4 (25 ppm)	10 ppm	14
rGO	22.1 (40 ppm)	5 ppm	15
MoS_2 thin films	8.1 (30 ppm)	0.3 ppm	16
Pt activated SnO_2	314.43 (1000 ppm)	50 ppm	17
Activated carbons	28 (500 ppm)	10 ppm	18
Modified SWCNT	27 (20 ppm)	0.1 ppm	19

rGo–WO_3 nanocomposites	1500 (100 ppm)	1.14 ppm	20
n-MoS_2/p-CuO	63 (500 ppm)	5 ppm	21
2D Ti_3C_2Tx	1 (100 ppm)	0.13 ppm	22
WS_2/TiO_2 QD	56.7 (500 ppm)	20 ppm	23
PADS	330 (40 ppm)	10 ppt	24

References

1. C. Huang, X. Shang, X. Zhou, Z. Zhang, X. Huang, Y. Lu, M. Wang, M. Löffler, Z. Liao, H. Qi, U. Kaiser, D. Schwarz, A. Fery, T. Wang, S. C. B. Mannsfeld, G. Hu, X. Feng, R. Dong, *Nat. Commun*. 2023, **14**, 3850.
2. Y. Lin, W. H. Li, Y. Wen, G. E. Wang, X. L. Ye, G. Xu, *Angew. Chem. Int. Ed*. 2021, **60**, 25758.
3. M. S. Yao, X. J. Lv, Z. H. Fu, W. H. Li, W. H. Deng, G. D. Wu, G. Xu, *Angew. Chem. Int. Ed*. 2017, **56**, 16510.
4. M. S. Yao, J. J. Zheng, A. Q. Wu, G. Xu, S. S. Nagarkar, G. Zhang, M. Tsujimoto, S. Sakaki, S. Horike, K. Otake, S. Kitagawa, *Angew. Chem. Int. Ed*. 2020, **59**, 172.
5. Z. Meng, R. M. Stolz, K. A. Mirica, *J. Am. Chem. Soc*. 2019, **141**, 11929.
6. N. Sharma, N. Sharma, P. Srinivasan, S. Kumar, J. B. B. Rayappan, K. Kailasam, *J. Mater. Chem. A* 2018, **6**, 18389.
7. N. A. Travlou, K. Singh, E. Rodríguez-Castellón, T. J. Bandosz, *J. Mater. Chem. A* 2015, 11417.
8. Z. Meng, A. Aykanat, K. A. Mirica, *J. Am Chem. Soc*. 2019, **14**, 2046.
9. X. Chen, Y. Lu, J. Dong, L. Ma, Z. Yi, Y. Wang, L. Wang, S. Wang, Y. Zhao, J. Huang, Y. Liu, *ACS Appl. Mater. Interfaces* 2020, **12**, 57235.
10. M. Shafiei, F. Hoshyargar, J. Lipton-Duffin, C. Piloto, N. Motta, A. P. O'Mullane, *J. Phys. Chem. C* 2015, **11**, 22208.
11. M. G. Campbell, D. Sheberla, S. F. Liu, T. M. Swager, M. Dinca, *Angew. Chem. Int. Ed*. 2015, **5**, 4349.
12. J. Zheng, K. Pang, X. Liu, S. Li, R. Song, Y. Liu, Z. Tang, *Adv. Funct. Mater.* 2020, **3**, 2005727.
13. M. Xue, F. Li, D. Chen, Z. Yang, X. Wang, J. Ji, *Adv. Mater*. 2016, **28**, 8265.
14. V. Mounasamy, G. K. Mani, D. Ponnusamy, K. Tsuchiya, A. K. Prasad, S. Madanagurusamy, *J. Mater. Chem. A* 2018, **6**, 6402.
15. L. T. Duy, T. Q. Trung, V. Q. Dang, B. U. Hwang, S. Siddiqui, I. Y. Son, S. K. Yoon, D. J. Chung, N. E. Lee, *Adv. Funct. Mater*. 2016, **2**, 4329.
16. V. Chabukswar, S. Pethkar, A. A. Athawale, *Sens. Actuators B Chem*. 2001, **77**, 657.
17. X. Liu, N. Chen, B. Han, X. Xiao, G. Chen, I. Djerdjc, Y. Wang, *Nanoscale* 2015, **7**, 14872.
18. N. A. Travlou, M. Seredych, E. Rodríguez-Castellón, T. J. Bandosz, *J. Mater. Chem. A* 2015, 3821.
19. L. A. Panes-Ruiz, M. Shaygan, Y. Fu, Y. Liu, V. Khavrus, S. Oswald, T. Gemming, L. Baraban, V. Bezugly, G. Cuniberti, *ACS Sens*. 2018, 79.
20. G. Jeevitha, R. Abhinayaa, D. Mangalaraj, N. Ponpandian, P. Meena, V. Mounasamy, S. Madanagurusamy, *Nanoscale Adv*. 2019, **1**, 1799.
21. S. Sharma, A. Kumar, N. Singh, D. Kaur, *Sensor Actuat B-Chem*. 2018, **275**, 499.
22. S. J. Kim, H. J. Koh, C. E. Ren, O. Kwon, K. Maleski, S. Y. Cho, B. Anasori, C. K. Kim, Y. K. Choi, J. Kim, Y. Gogotsi, H. T. Jung, *ACS Nano* 2018, **12**, 986.
23. Z. Qin, C. Ouyang, J. Zhang, L. Wan, S. Wang, C. Xie, D. Zeng, *Sensor Actuat B-Chem*. 2017, **253**, 1034.
24. J. Zhou, H. Lin, X. F. Cheng, J. Shu, J. H. He, H. Li, Q. F. Xu, N. J. Li, D. Y. Chen, J. M. Lu, *Mater. Horiz*. 2019, **6**, 554.